

## ANALYSIS OF A SOFT SWITCHED DUAL-BOOST CONVERTER

H. Donuk<sup>1</sup> I. Iskender<sup>2</sup> N. Genc<sup>3</sup>

1. *Electrical Engineering Department, Sirnak University, Sirnak, Turkey, hakan.donuk@gmail.com*  
2. *Electrical and Electronics Engineering Department, Gazi University, Ankara, Turkey, iresis@gazi.edu.tr*  
3. *Electrical and Electronics Engineering Department, Yuzuncu Yil University, Van, Turkey, nacigenc@gmail.com*

**Abstract-** This paper proposes a soft switched dual-boost converter using an auxiliary resonant circuit. The topology is composed of a general dual-boost converter and an auxiliary resonant circuit including one switch, inductor, capacitor and two diodes. The auxiliary resonant circuit helps the main switch to operate under ZVT condition. The auxiliary switch is also operated at soft switching mode. Furthermore, the proposed circuit removes the voltage stress on the main and auxiliary switches. Under soft switching conditions the efficiency of the converter increases. The converter has various advantages compared with the conventional boost converters as higher boost rate with low duty cycle, lower voltage stress on components and higher efficiency.

**Keywords:** Zero Voltage Transition, Dual-Boost Converter, Boost Converter, Soft Switching.

### I. INTRODUCTION

DC-DC converters controlled by Pulse Width Modulation technique have a wide range of application areas. Operating the converter at high frequency decreases the converter volume and increases the power density of converter. However, increasing the operating frequency increases the switching losses and the Electromagnetic Interference (EMI) resulting reduction in efficiency of converter [1]. Basically, switching losses are composed of switching losses of switches due to overlapping of voltage and current, loss of diodes due to reverse recovery phenomenon and discharge loss of the parasitic capacitor [2].

To reduce the switching losses several suppressing cells are made as RC/RCD, polar/non-polar, resonance/non-resonant and active/passive cells. The switching losses are greatly reduced by zero voltage switching method (ZVS) and the zero current switching (ZCS) method. There have been published many papers about boost converter with active soft-switching methods. Boost converter switching at zero voltage (ZVT) is one of the soft switching techniques given in [3]. There are methods given in [3], [4] and [5] in which the snubber cells cannot eliminate all the switching losses.

In [5-7] there are used multiple inductors that increase the volume and decrease the power density of the converter. Soft switching techniques used in [6] and [8]

reduces the losses but cannot remove the voltage stress of main and auxiliary switches. The turn on and turn off losses are reduced in [9], but due to several numbers of elements the volume of the converter increases. There is another study [10] in which auxiliary switch is used for soft switching. In the study given in [11] the active snubber circuit provides zero voltage transition modes for the main switch. There is no voltage and current stress on the main diode.

This paper proposes a soft switched dual-boost converter that is able to turn on both the active power switches at zero voltages to reduce their switching losses and evidently raise the conversion efficiency. In the study dual-boost converter circuit is operating under soft switching technique and the efficiency of the converter increases by reducing the switching losses. The problem of voltage stress is also eliminated. The operation principles of the converter and the conditions for realization of soft switching are analyzed in detail, simulation analysis performed using PSpice is given. The simulation results show that all the switches are operating at soft switching state and the efficiency of the converter is improved.

### II. CIRCUIT CONFIGURATION

Figure 1 represents the circuit configuration of the proposed dual-boost pulse width modulation (PWM) converter.

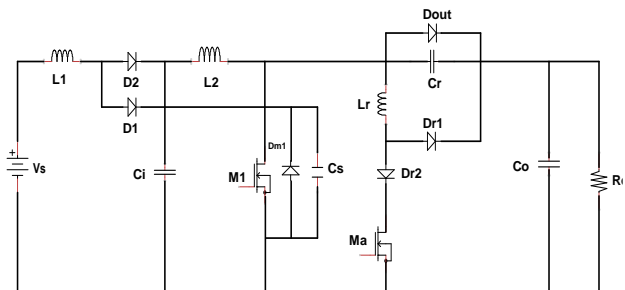


Figure 1. Proposed soft switched dual-boost DC/DC converter

The converter consists of one switch; two boost inductors  $L_1$  and  $L_2$ , two diodes  $D_1$  and  $D_2$ , and capacitors  $C_i$  and  $C_o$ . Except the output capacitance of the converter, the other components of the converter constitute the auxiliary circuit.  $M_a$ ,  $D_{r1}$ ,  $D_{r2}$ , and  $D_{out}$  represent the

auxiliary switch and diodes, respectively. The  $L_r$  and  $C_r$  present the inductor and capacitor of proposed auxiliary circuit, respectively. The  $D_{m1}$  is the intrinsic parallel diode of MOSFET  $M_1$  and the snubber capacitance,  $C_s$  is common for the main switch  $M_1$ .

### III. CIRCUIT OPERATION ANALYSIS

The following assumptions are made in analysis of the converter.

- The output capacitor  $C_o$  is large enough to neglect reasonably the output voltage ripple and consider a constant level output voltage.
- The forward voltage drops on MOSFET  $M_1$ ,  $M_a$  and diodes  $D_1$  and  $D_2$  are neglected.
- Inductors  $L_1$  and  $L_2$  are large and equal.
- The components of the converter are ideal.

The active switch,  $M_1$  is operated with pulse width modulation (PWM) control signals. This is gated with identical frequency and duty ratio. The operation of the converter can be divided into seven modes, the equivalent circuits and the theoretical waveforms are illustrated in above figures.

#### A. Mode 1

Prior to this mode, the main switch  $M_1$  and the auxiliary switch  $M_a$  are in the off state and output diode  $D_{out}$  is conducting. At the beginning of this mode,  $M_a$  is turned on. The resonant inductor ( $L_r$ ) current starts to rise through the path of  $V_s - L_1 - L_2 - L_r - M_a$ . Since the rise rate of this current is limited by  $L_r$ , the devices  $D_1$  and  $M_a$  are turned on under soft switching. The voltage across  $C_s$  is nearly equal to the output voltage ( $V_o$ ) in this interval and the initial voltage across the  $C_r$  is nearly equal to zero. During this time interval, the voltage across  $C_r$  and current of  $L_r$  can be expressed as [8],  $t_0 < t < t_1$ .

$$i_{L_r}(t) = \frac{V_{cs}}{L_r}(t_1 - t_0) = \frac{V_o}{L_r}(t - t_0) \quad (1)$$

$$V_{cr}(t) = 0 \quad (2)$$

$$(t_1 - t_0) = \Delta t_1 = \frac{i_{L1} x L_r}{V_o} \quad (3)$$

$$i_o(t) = i_{L1} - i_{C_i} - i_{L_r} \quad (4)$$

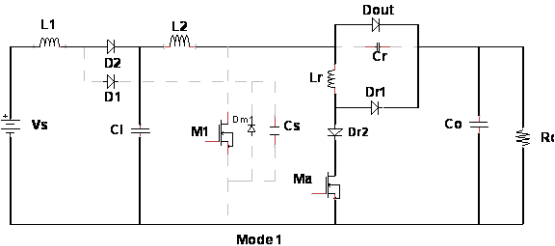


Figure 2. Equivalent circuit scheme of the operation mode 1 ( $t_0 < t < t_1$ )

#### B. Mode 2

$M_a$  current reaches  $i_{L1}$  and output current falls to zero at  $t = t_1$ . The snubber capacitor ( $C_s$ ) begins to discharge and the current in  $L_r$  increases because of the resonance between  $L_r$  and  $C_s$ .  $C_s$  is discharged until its voltage reaches zero at  $t_2$ . The resonant time period of this

interval, current of  $L_r$  and voltage across  $C_s$  are given by  $t_1 < t < t_2$ .

$$i_{L_r}(t) = i_{L1} + \frac{V_o}{Z} * \sin \omega (t - t_1) \quad (5)$$

$$V_{cs}(t) = V_o \cos \omega(t - t_1) \quad (6)$$

$$(t_2 - t_1) = \Delta t_2 = \frac{\pi}{2} \sqrt{L_r C_s} \quad (7)$$

where,  $\omega = \frac{1}{\sqrt{L_r C_s}}$  and  $Z = \sqrt{L_r C_s}$ .

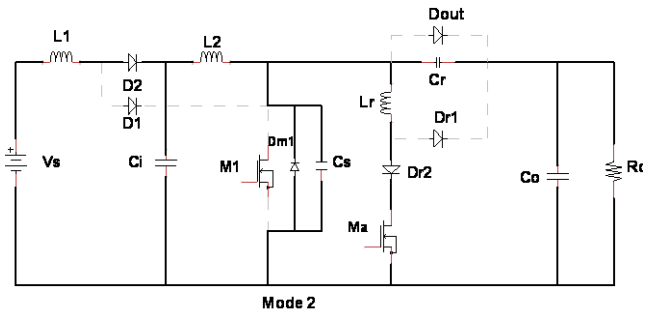


Figure 3. Equivalent circuit scheme of the operation mode 2 ( $t_1 < t < t_2$ )

#### C. Mode 3

At  $t = t_2$ , the main switch and  $D_2$  are in the off state and auxiliary switch and  $D_1$  are in the on state. Auxiliary switch conducts the current in  $L_r$ . As seen from the Figure 9 at the beginning of this mode current of snubber capacitor  $C_s$  is completely exhausted and the  $L_r$  current reaches its maximum rate. At this interval, the current in  $L_r$  flows in  $L_r - M_a$  and body diodes of the main switches. The voltage across  $C_r$  is discharged nearly to zero before  $t_2$ . The maximum current of  $L_r$  can be equated as [8]:

$$i_{L_r}(t) = i_{L_{r_{max}}} = i_{L1} + V_o / Z \quad (8)$$

$$V_{cr}(t) \approx 0 \quad (9)$$

At this mode, the main switch should be switched to satisfy the ZVT condition. By assuming the average inductor current of  $L_1$  is the half of the input current at steady state, delay time for  $M_1$ ,  $t_d$  can be expressed as [8]:

$$t_d = \Delta t_1 + \Delta t_2 = \frac{i_{in} x L_r}{V_o} + \frac{\pi}{2} \sqrt{L_r C_s} \quad (10)$$

Additionally, the current through inductors will start to increase linearly according to:

$$i_{L1} = \frac{V_s}{L_1 + L_r}(t_3 - t_2) \cong \frac{V_s}{L_1}(t_3 - t_2) \quad (11)$$

$$i_{L2} = \frac{V_{ci}}{L_2 + L_r} t \cong \frac{V_{ci}}{L_2} t \quad (12)$$

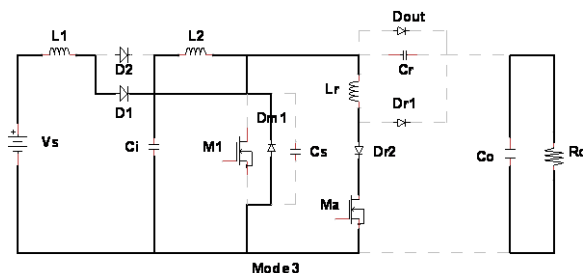


Figure 4. Equivalent circuit scheme of the operation mode 3 ( $t_2 < t < t_3$ )

**D. Mode 4**

As seen from the Figure 5 at the start of this interval,  $M_a$  is turned off and the main switch is turned on at the same time. At this mode, the main switches,  $M_1$  and  $L_r$  conduct the input current together. At the end of this mode the current of  $L_r$  and  $L_1, L_2$  reaches zero [12].

$$iL_1 = \frac{V_s - V_o}{L_1 + L_r} (t_4 - t_3) \cong \frac{V_s}{L_1} (t_4 - t_3) \tag{13}$$

$$iL_2 = \frac{V_{ci}}{L_2} (t_6 - t_4) \tag{14}$$

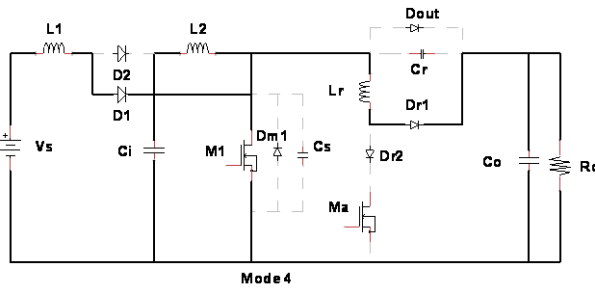


Figure 5. Equivalent circuit scheme of the operation mode 4 ( $t_3 < t < t_4$ )

**E. Mode 5**

This interval is composed of two equivalent circuit. The energy is stored in the boosting inductor  $L_1$  through the loop of  $V_s-L_1-D_1-M_1$  and stored in the boosting inductor  $L_2$  through the loop of  $C_i-L_2-M_1$ . The energy is transferred to the load through discharging capacitor,  $C_o$ .

The current of  $L_1$ :

$$iL_1 = \frac{V_s}{L_1} (t_5 - t_4) \tag{15}$$

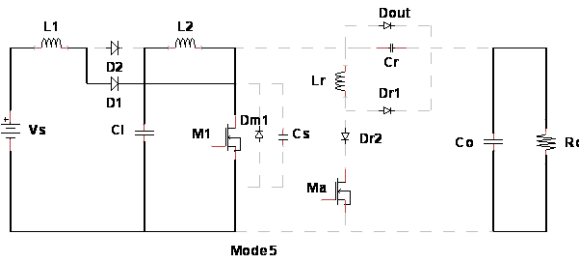


Figure 6. Equivalent circuit scheme of the operation mode 5 ( $t_4 < t < t_5$ )

**F. Mode 6**

At  $t_5$ , the current of main switch falls to zero and voltage across of  $M_1$  and  $C_s$  go up to output voltage  $V_o$ . At the end of this interval, the current of  $L_r$  starts to increase.

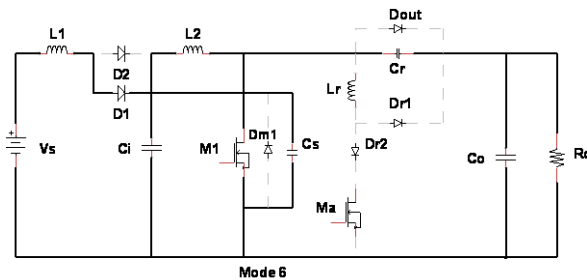


Figure 7. Equivalent circuit scheme of the operation mode 6 ( $t_5 < t < t_6$ )

**G. Mode 7**

At a certain moment  $t_6$ ,  $D_2$  and main switch are turned off.  $D_2, D_{r2}$  and  $D_{out}$  are turned on. The inductor currents  $I_{L1}$  and  $I_{L2}$  at that moment have reached peak values. The stored energy is supplied to load through diodes  $D_2, D_{r2}$  and  $D_{out}$ . As a result, the current through the inductors  $I_{L1}$  and  $I_{L2}$  will start to decrease linearly according to [12]:

$$iL_1 = \frac{V_s - V_{ci}}{L_1} (t_6 - t_7) \tag{16}$$

$$iL_2 = \frac{V_{ci} - V_o}{L_2 + L_r} (t_6 - t_7) \tag{17}$$

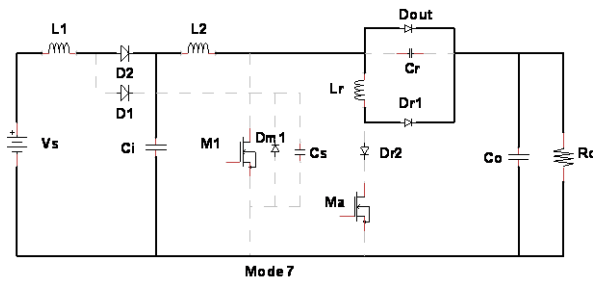


Figure 8. Equivalent circuit scheme of the operation mode 7 ( $t_6 < t < t_7$ )

Current  $C_i$  is inverted again, and  $C_i$  is now charging until  $D_1$  is turned on again and the cycle with its seven intervals is repeated.

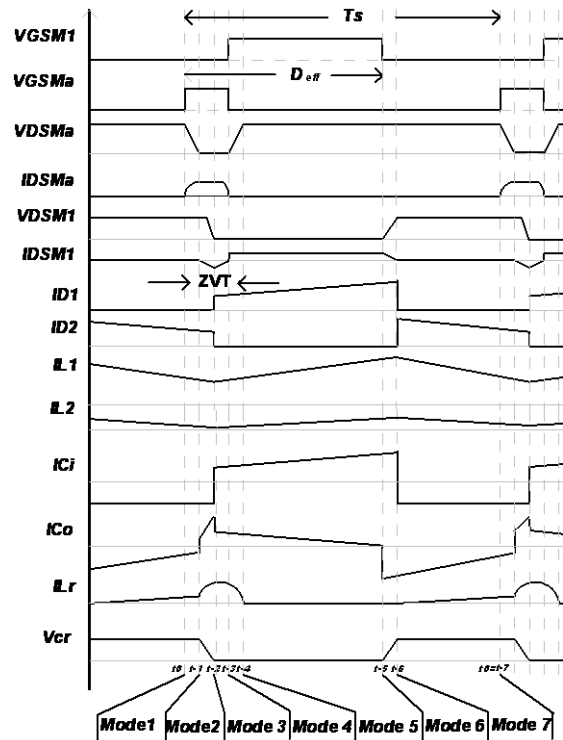


Figure 9. Theoretical waveforms of the proposed circuit topology

**IV. CIRCUIT DESIGN AND SELECTION OF COMPONENTS**

The dual-boost converter is a high-efficiency step-up DC/DC switching converter. The converter uses a switch to transfer power through pulse-width modulation technique.

This section presents a design procedure for the proposed soft switched dual-boost converter operating in continuous conduction mode (CCM). In the periodic switching scheme with period  $T$ , the average voltage across the first inductor must be zero. The relationship of voltage and current for first inductor is as [12]:

$$V_{L1} = L_1 \frac{di_{L1}}{dt} \quad (18)$$

$$I_{L1}(t) = \frac{1}{L_1} \int_0^t V_{L1}(t)dt + I_{L1}(0) \quad (19)$$

$$I_{L1}(t) = \frac{1}{L_1} \int_{t_0}^t V_{L1}(t)dt + I_{L1}(t_0) \quad (20)$$

$$I_{L1}(T+t_0) = \frac{1}{L_1} \int_{t_0}^{T+t_0} V_{L1}(t)dt + I_{L1}(t_0) \quad (21)$$

$$I_{L1}(T+t_0) - I_{L1}(t_0) = \frac{1}{L_1} \int_{t_0}^{T+t_0} V_{L1}(t)dt \quad (22)$$

where,  $I_{L1}(t) = I(T+t)$ ,  $t = t_0$ ,  $V_{L1}(t) = \frac{1}{L_1} \int_{t_0}^{T+t} V_{L1}(t)dt = 0$ .

According to the voltage second product:

$$V_s t_{on} = (V_{ci} - V_s) t_{off} \quad \text{or} \quad V_s T = (V_{ci}) t_{off} \quad (23)$$

$$V_{ci} = \frac{T}{t_{off}} V_s = \frac{T}{T - t_{on}} V_s \quad (24)$$

$$V_{ci} = \frac{1}{1 - (D_{aux} + D_{main})} V_s \quad (25)$$

where,  $D_{eff} = D_{aux} + D_{main}$ ,  $D_{main}$  is duty cycle of the main switch and  $D_{aux}$  is the duty cycle of the auxiliary switch.

The same procedure is used to find the relation between output voltage  $V_o$  and the first stage output  $V_{ci}$ :

$$(V_{ci}) t_{on} = (V_o - V_{ci}) t_{off} \quad (26)$$

$$V_{ci} (t_{on} + t_{off}) = (V_o) t_{off} \quad (27)$$

$$V_o = \frac{T}{t_{off}} V_{ci} = \frac{T}{T - t_{on}} V_{ci} \quad (28)$$

$$V_o = \frac{1}{1 - (D_{aux} + D_{main})} V_{ci} = \frac{1}{(1 - D_{aux} + D_{main})^2} V_s \quad (29)$$

$$V_o = \frac{1}{1 - D_{eff}} * V_{ci} = \frac{1}{(1 - D_{eff})^2} * V_s \quad (30)$$

The gain of the dual-boost DC-DC converter will be [12]:

$$V_o = \frac{1}{(1 - D_{eff})^2} * V_s \quad (31)$$

To achieve the zero voltage transition, a delay time ( $T_{delay}$ ) of main switch PWM is required. The minimum delay time must be satisfied the following equation. The time is consisted of the resonant time between  $L_r$  and  $C_s$  and the time that the resonant inductor current equals the input current.

$$T_d \geq \frac{i_{in} x L_r}{V_o} + \frac{\pi}{2} \sqrt{L_r C_s} \quad (32)$$

It is seen from Equation (32) that  $T_d$  depends on  $V_o$ ,  $I_{in}$ ,  $L_r$  and  $C_s$ . During the delay time, the auxiliary switch is turned on. The input current ripple  $\Delta I_L$  on each of the boost inductors can be denoted as [13]:

$$\Delta i_{L1} = \frac{V_s x D_{eff}}{f_{sx} L_1} \quad (33)$$

$$\Delta i_{L2} = \frac{V_s x D_{eff}}{f_{sx} (1 - D_{eff}) x L_2} \quad (34)$$

Input and output capacitors voltage ripple can be determined as [13]:

$$\Delta V_{ci} = \frac{i_o x D_{eff}}{f_{sx} (1 - D_{eff}) x C_i} \quad (35)$$

$$\Delta V_{co} = \frac{i_o x D_{eff}}{f_{sx} C_o} \quad (36)$$

The corresponding steady-state operating condition is given by [14]:

$$V_{ci} = \frac{E}{(1 - D_{eff})} \quad , \quad V_{co} = \frac{E}{(1 - D_{eff})^2} \quad (37)$$

$$i_{L1} = \frac{E}{(1 - D_{eff})^4 R_o} \quad , \quad i_{L2} = \frac{E}{(1 - D_{eff})^3 R_o}$$

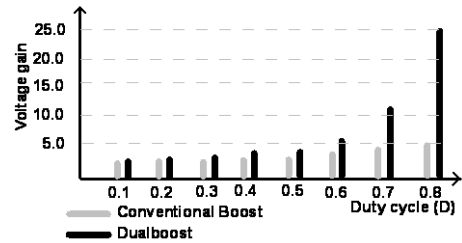


Figure 10. Voltage conversion ratio

The voltage conversion difference between conventional boost and dual boost can be seen from the Figure 10. It can be noted that high voltage gain values are obtained with a low duty cycle, as theoretically expected [12].

## V. SIMULATION RESULTS

In this section, simulations are carried out to verify the theoretical analysis given in the previous sections. Since the PSpice simulation program includes models of the real components, the proposed topology is firstly simulated via this program and the simulation results of the proposed topology are shown in the following figures. The components and parameters used in the simulation studies are summarized in Table 1.

Table 1. Components used in the simulations

Components	Symbols	Parameters
Input voltage	$V_{source}$	100 V
Output voltage	$V_{output}$	300 V
Switching frequency	$f_{sw}$	50 kHz
Main inductances	$L_1$ and $L_2$	300 uH
Auxiliary inductance	$L_r$	1 uH
Auxiliary capacitance	$C_r$	5 nF
Snubber capacitance	$C_s$	1 nF
Input capacitance	$C_i$	30 uF
Output capacitance	$C_o$	50 uF
Main switch	$M_1$	IRF250-30A
Auxiliary switch	$M_a$	IRF350-14A
Main diodes	$D_1$ and $D_2$	MUR810
Auxiliary diodes	$D_{r1}$ , $D_{r2}$ , $D_{out}$ and $D_{m1}$	MUR810
Output power	$P_o$	600 W

The converter design specifications are considered for medium power sources. Since the output voltage generated by the photovoltaic arrays and the fuel stack sources is relatively low, their output voltage is generally increased via conventional boost or dual-boost type dc-dc converters to the required voltage level. The converter specifications consist of:

- Output power  $P_o = 600 \text{ W}$
- Output voltage ripple  $\Delta V_o = 2\%$
- Input current ripple  $\Delta I_L = 15\%$
- Switching frequency  $f_s = 50 \text{ kHz}$

As seen from Figure 14, delay time is less than 5% of the switching period during which ZVT action is performed.

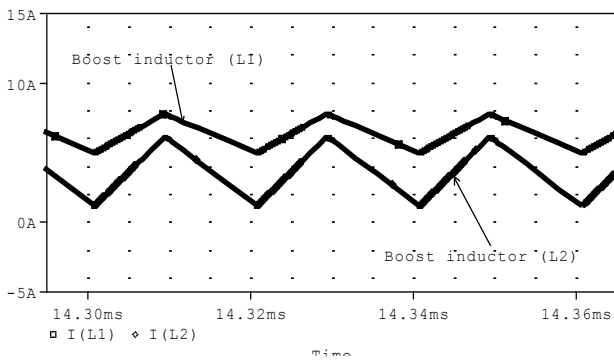


Figure 11. Simulation waveforms of the current of inductors ( $I_{L1}$ ,  $I_{L2}$ )

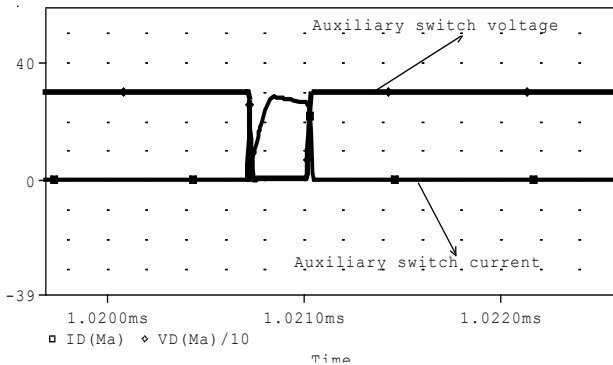


Figure 12. Simulation waveforms of the voltage and current of the auxiliary switch  $M_a$  ( $V_{DMa}/10$ ,  $I_{DMa}$  and  $P_o = 600 \text{ W}$ ,  $V_o = 300 \text{ V}$ )

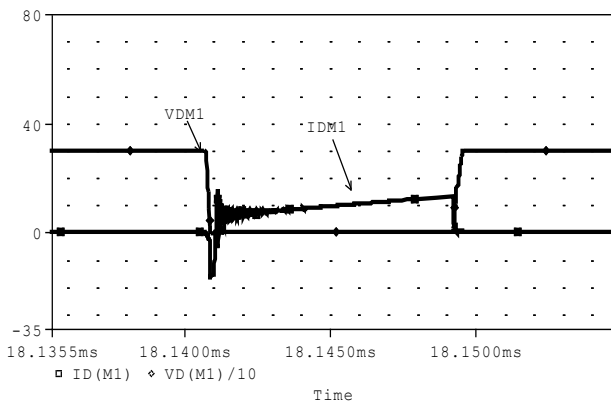


Figure 13. Simulation waveforms of the voltage and current of the main switch  $M_1$  ( $V_{DM1}/10$ ,  $I_{DM1}$ ) under soft switching condition ( $P_o = 600 \text{ W}$ ,  $V_o = 300 \text{ V}$ )

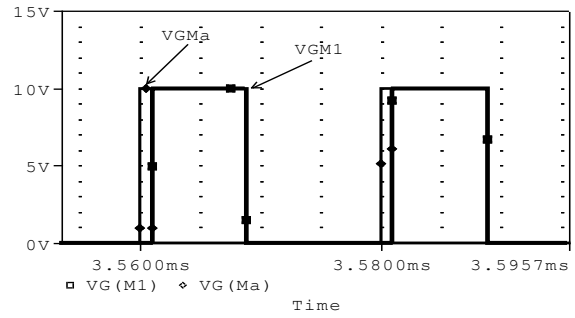


Figure 14. Simulation waveforms of the control signal of the main switch ( $M_1$ ) and auxiliary switch ( $M_a$ ) ( $P_o = 600 \text{ W}$ ,  $V_o = 300 \text{ V}$ )

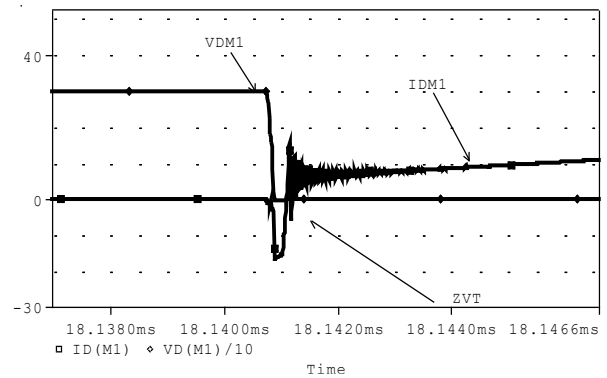


Figure 15. Simulation waveforms of the voltage and current of the main switch  $M_1$  ( $V_{D1}/10$ ,  $I_{DM1}$ ) under soft switching condition turn on ( $P_o = 600 \text{ W}$ ,  $V_o = 300 \text{ V}$ )

From the simulation results given in Figures 15 and 16, it is seen that the main switch  $M_1$  is turned on perfectly with ZVT and turned off under near ZCS. Figure 12 shows auxiliary switch,  $M_a$  which is turned on and off under soft switching.

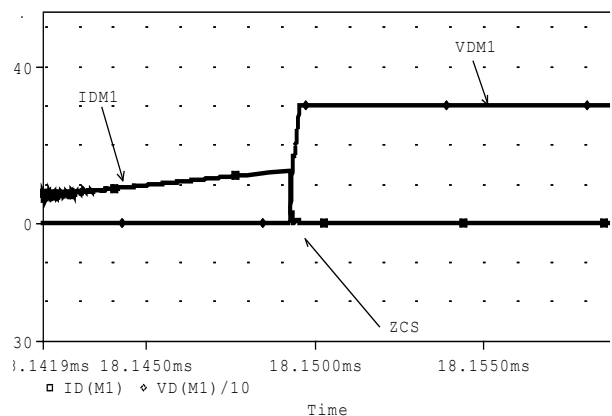


Figure 16. Simulation waveforms of the voltage and current of the main switch  $M_1$  ( $V_{DM1}/10$ ,  $I_{DM1}$ ) under soft switching condition turn off ( $P_o = 600 \text{ W}$ ,  $V_o = 300 \text{ V}$ )

In addition, the devices  $D_1$ ,  $D_2$ ,  $D_{r1}$ ,  $D_{r2}$  and  $D_{out}$  operate under soft switching conditions. The losses of the semiconductor devices and total efficiencies of the circuits for hard switching and the proposed soft switching cases are summarized for various loads as given in Table 2.

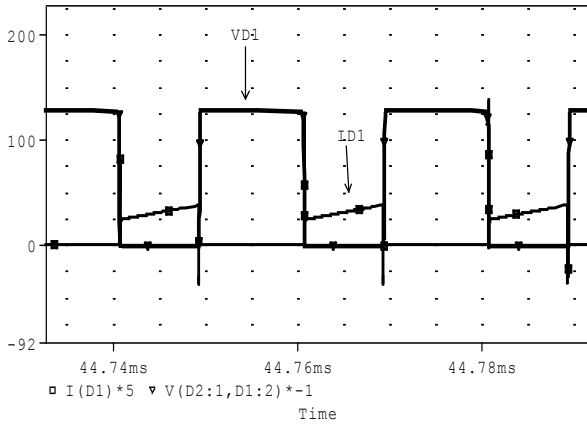


Figure 17. Simulation waveforms of the voltage and current of the main diode  $D_1$  ( $V_{D1}$ ,  $I_{D1} \times 5$ ) under soft switching condition ( $P_o = 600$  W,  $V_o = 300$  V)

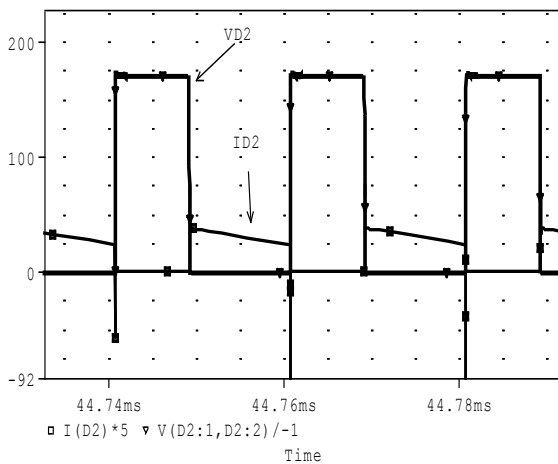


Figure 18. Simulation waveforms of the voltage and current of the main diode  $D_2$  ( $V_{D2}$ ,  $I_{D2} \times 5$ ) under soft switching condition ( $P_o = 600$  W,  $V_o = 300$  V)

The switching operations of the main, output diode and auxiliary circuit diodes are observed via simulation studies. It is observed that the main, output diode and auxiliary circuit diodes turn on and turn off under soft switching and there is no voltage stress on the diodes. The simulation results are in very close agreement and verify the theoretical studies given in section III. From the simulation result given in Figure 20, it is seen that the output voltage ripple is at a level acceptable.

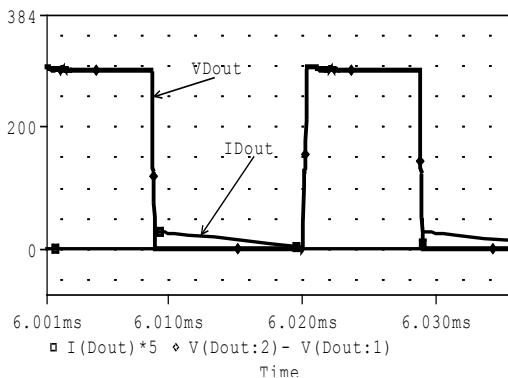


Figure 19. Simulation waveforms of the voltage and current of the output diode  $D_{out}$  ( $V_{Dout}$ ,  $I_{Dout} \times 5$ ) under soft switching condition ( $P_o = 600$  W,  $V_o = 300$  V)

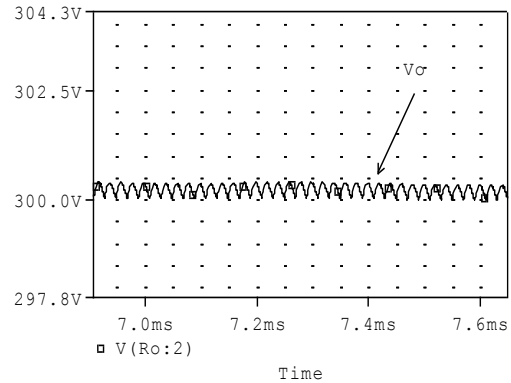


Figure 20. Simulation waveforms of the output voltage ( $V_o$ ) ( $P_o = 600$  W,  $V_o = 300$  V,  $D_{eff} = 0.422$ )

Table 2. Losses of the semiconductor devices and total efficiencies of the circuits in hard switching and the proposed soft switching converter

$V_s = 100$ V, $V_o = 300$ , Frequency = 50 kHz							
DC-DC Dual Boost Converter							
Load %	Hard or soft	Power Losses			Input power	Output power	Efficiency %
		Main switch	Auxiliary switch	Diodes and others			
20	Hard	3.3	None	7.3	130.6	120	91.8
	Soft	1.1	1.95	8	11.1	120	91.5
25	Hard	4	None	5.4	159.4	150	94.10
	Soft	1	2	5.8	161.6	150	92.8
50	Hard	7.6	None	7.8	315.4	300	95.1
	Soft	3.4	4.7	9	317.1	300	94.60
75	Hard	13.2	None	9.1	472.3	450	95.2
	Soft	5.4	8.1	6.5	470	450	95.75
100	Hard	20.3	None	10.8	631.1	600	95
	Soft	9.2	9.27	8.3	626.7	600	95.7

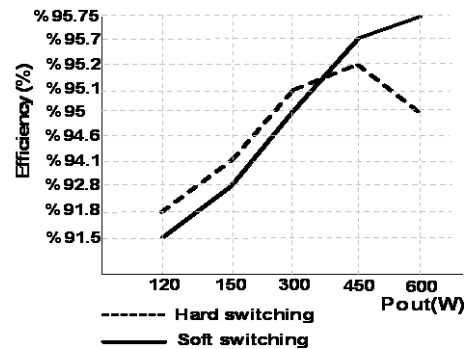


Figure 21. Overall efficiency curves of the hard switching and the proposed soft switching converters comparatively

At 450 W output power in the hard switching operation the main switch loss is about 13.2 W and this loss is equal 59.1% of total loss of circuit. At 450 W output power in proposed soft switching converter, the main switch loss is about 5.4 W and this loss is equal 27% of total circuit loss.

## VI. CONCLUSIONS

In this paper, a soft switched dual-boost converter using an auxiliary resonant circuit is proposed. Operation modes are divided considering the voltage and current waveforms. Equivalent circuit of each operation mode is illustrated and the current paths are indicated.

Each mode is analyzed through the simulation. It is verified that the main switch operates at soft switching. The main switch is turned on with ZVT and turned off under near ZCS. The auxiliary switch turned on and turned off under the soft switching mode.

In addition, the main diodes and auxiliary diodes turn on and off under soft switching cases. It can be clearly seen that the predicted operation principles and analysis of the proposed converter are verified with all of the simulation results. In the proposed converter, most of the drawbacks of the conventional ZVT converter are overcome both perfectly and easily. All the semiconductor devices of the converter are both turned on and off under soft switching state. There is no any additional voltage and current stresses on main devices and the auxiliary devices.

### NOMENCLATURES

- $\Delta I_{L1}$ : Input current ripple of  $L_1$
- $\Delta I_{L2}$ : Input current ripple of  $L_2$
- $\Delta V_{ci}$ : Voltage ripple of  $C_i$
- $\Delta V_{co}$ : Output voltage ripple of  $C_o$
- Z: Impedance of the auxiliary circuit
- $D_{eff}$ : Effective duty cycle rate

### REFERENCES

[1] W. Huang, G. Moschopoulos, "A New Family of Zero-Voltage-Transition PWM Converters with Dual Active Auxiliary Circuits", IEEE Transactions on Power Electronics, Vol. 21, pp. 370-379, 2006.

[2] I. Aksoy, "A New Soft-Switched PWM DC-DC Converter Design, Analysis and Application", Ph.D. Thesis, Sciences Institute, Yildiz Technical University, Istanbul, Turkey, 2007.

[3] G. Hua, C. Leu, Y. Jiang, F. Lee, "Novel Zero Voltage Transition PWM Converters", IEEE Transaction on Power Electronics, Vo. 9, No. 2, pp. 213-219, 1994.

[4] H. Bodur, A.F. Bakan, "A New ZVT-PWM DC-DC Converter", IEEE Transactions on Power Electronics, Vol. 17, No. 1, pp. 40-47, 2002.

[5] M. Phattanasak, "A ZVT Boost Converter Using an Auxiliary Resonant Circuit", PEDES'06 International Conference on Power Electronics, Drives and Energy Systems, pp. 1-6, 12-15 Dec. 2006.

[6] A.F. Bakan, H. Bodur, I. Aksoy, "A Novel ZVT-ZCT-PWM DC-DC Converter", 11th European Conference on Power Electronics and Applications (EPE2005), Dresden, pp. 1-8, Sept. 2005.

[7] R. Gurunathan, A.K. Bhat, "ZVT Boost Converter Using a ZCS Auxiliary Circuit", IEEE Trans. Aerosp. Electron. Syst., Vol. 37, No. 3, pp. 889-897, July 2001.

[8] I. Iskender, N. Genc, "Design and Analysis of a Novel Zero-Voltage-Transition Interleaved Boost Converter for Renewable Power Applications", International Journal of Electronics, Vol. 97, pp. 1051-1070, DOI: 10.1080/00207217.2010.482021.

[9] N. Jain, P. Jain, G. Joos, "Analysis of a Zero Voltage Transition Boost Converter Using a soft Switching Auxiliary Circuit with Reduced Condition Losses", IEEE PESC Conference Record, Vol. 4, pp. 1799-1804, 2001.

[10] R. Gurunathan, A.K.S. Bhat, "A Zero-Voltage-Transition Boost Converter Using a Zero Voltage Switching Auxiliary Circuit", IEEE Transactions on Power Electronics, Vol. 17, pp. 658-668, 2002.

[11] H. Bodur, A.F. Bakan, "A New ZVT-ZCT-PWM DC-DC Converter", IEEE Trans. on Power Electron, Vol. 19, No. 3, pp. 676-684, 2004.

[12] S. Khairy, A. Mazen, A. Adel, A. Mahmoud, "New High Voltage Gain Dualboost DC-DC Converter for Photovoltaic Power Systems", Electric Power Components and Systems, Vol. 40, pp. 711-728, 2012.

[13] J. Leyva Ramos, M.G. Ortiz Lopez, J.A. Morales Saldana, L.H. Diaz Saldierna, "Switching Regulator Using a Quadratic Boost Converter for Wide DC Conversion Ratios", IET Power Electronics, Vol. 2, No. 5, pp. 605-613, 2009.

[14] J.A. Morales-Saldana, R. Galarza Quirino, J. Leyva Ramos, E.E. Carbajal Gutierrez, M.G. Ortiz Lopez, "Multiloop Controller Design for a Quadratic Boost Converter", IET Electronic, Power Appl., Vol. 3, pp. 362-367, 2007.

### BIOGRAPHIES



**Hakan Donuk** was born in Diyarbakir, Turkey, 1987. He received the B.Sc. degree in Electrical Engineering from Dicle University, Diyarbakir, Turkey and is currently working on his M.Sc. thesis in Gazi University, Ankara, Turkey. He is currently a Lecturer at Sirnak University, Sirnak, Turkey. His research areas include soft switching, active-passive snubber cells in power electronics, renewable energy.



**Ires Iskender** received his M.Sc. and Ph.D. degrees in Electrical and Electronics Engineering from Middle East Technical University, Ankara, Turkey in 1990, 1996, respectively. He is currently a Professor in Department of Electrical and Electronics Engineering, Gazi University, Ankara, Turkey. His research interests include power electronic, renewable energy, intelligent control, electrical machine, power quality, power transformers.



**Naci Genc** completed his B.Sc. degree in Electrical Education Department from Gazi University, Ankara, Turkey. He received his M.Sc. degree from Electrical and Electronics Engineering Department, Yuzuncu Yil University, Van, Turkey and Ph.D. degree from Electrical and Electronics Engineering Department, Gazi University, in 2002 and 2010, respectively. From 1999 to 2010, he worked as a Research Assistant in Electrical and Electronics Engineering Department of Yuzuncu Yil University, Middle East Technical University and Gazi University, Turkey. He is currently an Associate Professor at Yuzuncu Yil University. His research interests include power electronics, electrical machines, renewable energy, solar photovoltaic energy systems and control systems.